Was the observed pre-seismic total electron content enhancement a true precursor of the 2011 Tohoku-Oki Earthquake?

R. Ikuta[1], T. Hisada[1], G. Karakama[2] and O. Kuwano[3]

[1]Faculty of Science, Shizuoka University, Japan.
[2]Graduate School of Environmental Studies, Nagoya University, Japan.
[3]JAMSTEC, Japan.

Corresponding author: Ryoya Ikuta (ikuta.ryoya@shizuoka.ac.jp)

Key Points:

- Ionospheric TEC enhancement occurs so often without earthquakes, which can explain the "precursors" as just a product of chance
- A large TEC depletion spreading 500 km in diameter and lasting at least 120 minutes after the Tohoku-Oki earthquake
- Excluding window is in danger of mistaking the post-seismic depletion for a preseismic enhancement

Abstract

Here we test the precursory enhancement in ionospheric total electron content (TEC) which has been reported by Heki (2011) and numerous Global Navigation Satellite System (GNSS) TEC observational studies before the 2011 Mw9.0 Tohoku-Oki and many great earthquakes. We verify the frequency of this TEC enhancement via analysis of a two-month vertical TEC (VTEC) time series that includes the Tohoku-Oki Earthquake using the procedure, based on Akaike's information criterion, and threshold of Heki and Enomoto (2015). The averaged occurrence rate of the TEC enhancement is much larger than that reported by Heki and Enomoto (2015) when all

of the visible GPS satellites at a given station are taken into account. We cannot rule out the possibility that the pre-seismic VTEC changes before the great earthquakes that were reported by Heki and Enomoto (2015) are not precursors but just a product of chance. We also analyze the spatial distribution of the pre-seismic TEC enhancement and co-seismic TEC depletion for the Tohoku-Oki Earthquake with the data after reducing inter-trace biases. We observe significant post-seismic depletion that lasted at least 2 h after the earthquake and extended at least 500 km around the center of the large-slip area. This means that evaluation of the enhancements using reference curves which was adopted by Heki 2011 and even by the recent papers (e.g. He and Heki 2016, 2017, 2018) is in danger of mistaking a large and long-lasting post-seismic TEC depletion for a pre-seismic enhancement.

1 Introduction

Precursory enhancement of the ionospheric total electron content (TEC) within a few tens of minutes before large earthquakes has been reported by Heki (2011) and numerous Global Navigation Satellite System (GNSS) TEC observational studies (e.g., Heki and Enomoto, 2013; Heki and Enomoto, 2015; He and Heki, 2016, 2017, 2018). Heki (2011) extracted the TEC enhancement prior to the 2011 Tohoku-Oki Earthquake using a reference curve to model the slant TEC (STEC) time series, with the departure from the reference curve defining the TEC anomaly in the focal area. He excluded a 48-min time window surrounding the mainshock (from 34 min before to 14 min after the mainshock) from the STEC time series to deduce the reference curve, and showed that the residual STEC began to increase 40 min before the earthquake, returning to the normal state when the post-seismic acoustic wave reached the ionosphere (Heki, 2011). However, this approach has received criticism (e.g., Kamogawa and Kakinami, 2013; Masci et al., 2015). Kamogawa and Kakinami (2013) attributed the TEC enhancement reported by Heki (2011) to an artifact caused by the combined effects of TEC disturbances under active geomagnetic conditions and an ionospheric hole generated by a tsunami. Heki and Enomoto (2013) revisited the data to address this criticism, and claimed that the tsunami did not make an ionospheric hole since their pre-seismic increase in the vertical TEC (VTEC) was comparable to the post-seismic decrease. They suggested that the post-seismic decrease was due to the recovery from the precursory TEC enhancement, rather than a post-seismic tsunamigenic hole (Heki and

Enomoto, 2013). This interpretation justifies the exclusion of the time window immediately surrounding the mainshock, for which the end time is generally set at 20 min after the mainshock, in deducing the reference VTEC curves in subsequent studies (e.g. He and Heki, 2016, 2017, 2018). However, He and Heki (2017) also considered the possibility of a post-seismic hole when they studied the pre-seismic enhancement of Mw 7–8 earthquakes using the reference curves. They claimed that the post-seismic TEC depletions should be spatially limited above the focal area, even if they persist for a while, such that excluding the ±30-min time window surrounding the earthquake is enough to avoid these effects because the ionospheric penetration point (IPP) along the line of sight (LOS) between a station and satellite can pass through the area within this period (He and Heki, 2017). In addition to these rebuttals, Heki and Enomoto (2015) detected a positive break in the TEC time series (sudden increase in the TEC rate) without using reference curves before five great earthquakes based on Akaike's information criterion (AIC). They claimed that whether this positive break is space weather origin or not could be judged stochastically, even though the propagation of the positive break resembles a large-scale traveling ionospheric disturbance (LSTID) and there were active geomagnetic conditions during the period surrounding the 2011 Tohoku-Oki Earthquake (Heki and Enomoto, 2015). They detected positive breaks for five of the eight analyzed Mw 8.2–9.2 earthquakes exceeding their TEC unit (TECU) threshold (3.0 TECU/h). They showed that the probability of the random occurrence of such breaks was below 1/10 per hour, which was the averaged frequency over the three-week period surrounding the 2011 Tohoku-Oki Earthquake. They then showed that the detection probability of such breaks during the 1.5-h period before the five earthquakes would be $(1.5 \times 1/10)^5$, which is too small to be considered a fortuity. However, their sampling approach would have underestimated the occurrence rate if the TEC enhancement varied between different satellites, since they only used one satellite to demonstrate the occurrence rate of the break.

Here we first test the occurrence rate of the TEC break using all of the visible satellites during a 61-day period surrounding the 2011 Tohoku-Oki Earthquake. And then we also study the spatio-temporal characteristics of the TEC breaks. We then observe the post-seismic VTEC depletion at the time of the Tohoku-Oki Earthquake using data after reducing inter-trace biases, by which we study the potential risk in using the reference curve to estimate TEC enhancements.

2 TEC data processing

We calculated the VTEC time series from the L1 and L2 carrier phases of the global positioning system (GPS) signal for each GNSS station–satellite pair of the GNSS Earth Observation Network (GEONET) by implementing the following procedures.

2.1 Convert the geometry-free linear combination (L4) into the TEC deviation (ΔTEC)

We first obtained the phases of the L1 and L2 signals to calculate the carrier phase geometry-free combination (L4). We removed the cycle slips from L4 based on its jump, and then shifted L4 to fit the geometry-free linear combination between the C1 and P2 codes to remove the phase ambiguities. This shifted L4 was multiplied by a constant $\frac{10^{-16} f_1^2 f_2^2}{40.308(f_1^2 - f_2^2)}$, where f_1 and f_2 are the dominant frequencies of the L1 and L2 signals, respectively, to obtain the TEC deviation (ΔTEC). ΔTEC is measured in TECU, where 1 TECU is equivalent to 10^{16} electrons m^{-2}, which also corresponds to 0.162 m and 0.2675 m of the L1 and L2 signal delays, respectively.

The inter-frequency biases (IFBs) of the stations and differential code biases (DCBs) of the satellites are both included in the ΔTEC data. We corrected for these biases to obtain meaningful slant TEC (STEC) values as follows:

$$STEC_{ij}(t) = \Delta TEC_{ij}(t) - DCB_j - IFB_i, \quad (1)$$

where t is the time, and DCB_j and IFB_i correspond to the j-th satellite and i-th receiver, respectively. STEC was then converted to VTEC as follows:

$$VTEC_{ij}(t) = STEC_{ij}(t)\, cos\psi_{ij}(t), \quad (2)$$

where ψ_{ij} is the incident angle of the signal which penetrate a thin ionosphere at IPP at 300 km above the ground.

The satellite's DCBs between C1 and P2 were calculated from the P1–C1 and P1–P2 code biases provided by the University of Bern (ftp://ftp.aiub.unibe.ch/). The receiver's IFBs between C1 and P2 were provided by the Electronic Navigation Research Institute (ENRI) (Sakai, 2005).

2.2 TEC break detection

Heki and Enomoto (2015) evaluated the occurrence rate of the TEC enhancement in the VTEC time series using only one station–satellite pair; we followed their methodology here. A moving window was adopted that fit a pair of lines to the VTEC curve, with the break between the two lines set at the middle of the window. The significance of the break on the fit was determined by calculating the difference of AIC value between the two lines with break and a single line that was fit to the entire VTEC curve in the window. This difference was denoted as $-\Delta$AIC; a pair of lines was judged to provide a better fit to the VTEC curve than a single line when $-\Delta$AIC was positive. The TEC enhancement was then evaluated by comparing the increase in slope of the latter line to that of the former line when $-\Delta$AIC was positive. The break was regarded as a "significant positive break" when the increase in slope between the two linear fits exceeded a certain threshold. Here we expand the approach of Heki and Enomoto (2015) by applying this procedure to all of the visible satellites from GNSS station 3009 instead of using only a single satellite–station pair (They used only PRN15). This approach is more reasonable to simulate the situation that a precursor seeker can choose any one of all visible satellites when they look for a positive break prior to a great earthquake. We adopt a ±30-min time window and regard an increase that is larger than 3.0 TECU/h (absolute) and 75% of the original rate (relative) as a significant positive break, following Heki and Enomoto (2015).

3 Results: Spatiotemporal distribution of positive breaks

Figure 1 shows the VTEC time series for the three-week period surrounding the 2011 Tohoku-Oki Earthquake, using the same dataset as Heki and Enomoto (2015) (satellite PRN15 and GNSS station 3009); the time series looks similar to that in figure 6 of Heki and Enomoto (2015). Positive breaks are detected seven times (red dots in Figure 1), including the pre-seismic break before the Tohoku-Oki Earthquake, as observed by Heki and Enomoto (2015). The two breaks just after the Tohoku-Oki Earthquake are not taken into account here (gray dots in Figure 1), as they were mentioned by Heki and Enomoto (2015).

We apply this analysis to the 61-day VTEC time series from 9 February (DOY40) to 10 April 2011 (DOY100). The positive break rate should have been accurately evaluated by Heki

and Enomoto (2015) if it was simultaneously observed by all of the visible satellites. However, their positive break rate, which was evaluated using only one satellite, would be an underestimate if it was independently observed by each satellite because they would have missed positive breaks that occurred at satellites other than PRN15 at different times in the study period.

Figure 2a shows the number of detected significant positive breaks during the daytime (12:00–17:00 local time (LT); 03:00–08:00 UTC) for each day within the 61-day period. The breaks are calculated using all of the visible satellites with an elevation angle higher than 25°. If a period where the slope exceeds the threshold overlapped with a period from one or more other satellites, then these periods are regarded as one event. A total of 198 positive break events are detected within the 305-h observation period, resulting in an averaged occurrence rate of 0.65 times per hour. Approximately 36% of the breaks are detected simultaneously by multiple satellites, with the remaining 64% detected by one satellite (Figure 2b). The positive break 40 min before the Tohoku-Oki Earthquake is detected by two satellites (PRN15 and 26) from the station 3009.

The diurnal variations in Figure 2c show that the occurrence rate of the positive break is higher in the daytime (09:00–17:00 LT; 00:00–08:00 UTC) and early morning (05:00–07:00 LT; 20:00–22:00 UTC). Positive breaks are detected about three times more frequently during the daytime than in the predawn hours (02:00–05:00 LT; 17:00–20:00 UTC), which is explained by variations in the background VTEC level. The high rate of break detection in the early morning is explained by TEC enhancement at dawn.

The positive break detection is also highly dependent on the LOS configuration. Figure 3a shows the spatial distribution of the detection rate of breaks at sub-ionospheric points (SIPs), which is calculated by dividing the number of detected positive breaks by the SIP density. More positive breaks tend to be detected when the satellites are at a lower elevation angle. The detection rate is very high when the elevation is below 20°, especially in the southern sky. Figure 3b shows the relationship between the elevation mask and number of detected TEC breaks. The number of detected events is proportional to the number of satellites in view when the elevation mask angle is larger than 35°. However, the number of detected events increases much more rapidly than the number of satellites in view when the elevation mask angle is less than 35°. This trend should be due to unstable VTEC behavior in the low-angle LOS, as in this case the ray paths travel longer distances through the ionosphere. When a 35° elevation mask angle is

175 applied, a total of 102 positive TEC breaks are detected during the 61-day period (305 hours).
176 Each satellite detects an average of 21–22 breaks during the 61-day period with elevation mask
177 angle of 35° (Figure 3c). This detection rate is similar to that in Heki and Enomoto (2015), where
178 seven breaks were detected with satellite PRN15 over a 21-day period. Therefore, the occurrence
179 rate of positive breaks considering all satellites in view is about five times larger than that Heki
180 and Enomoto (2015) observed.

181 **4 Discussion**

182 The results of the stochastic TEC evaluation illustrate that the significant positive breaks
183 are observed much more often than reported by Heki and Enomoto (2015). The average
184 occurrence rate of the TEC positive breaks measured under the same conditions and threshold as
185 those of Heki and Enomoto (2015), and the inclusion of all of the visible satellites, is 0.33 times
186 per hour with a 35° elevation mask angle. This occurrence rate seems not enough low to rule out
187 the possibility of product of chance for pre-seismic positive TEC breaks. Furthermore,
188 considering that they adopted even lower elevation mask angles in detecting the pre-seismic
189 enhancement for some earthquakes, the expected occurrence rate would be even higher than it.
190 Here we first evaluate the probability of the positive TEC breaks observed as just a product of
191 chance before the five of eight great earthquakes reported by Heki and Enomoto (2015) considering the
192 applied elevation mask angles. We then test some of the basis for precursor that Heki (2011) and his
193 group have presented, based on the spatiotemporal VTEC distribution before and after the 2011 Tohoku-
194 Oki Earthquake.

195 **4.1 Probability of the pre-seismic breaks**

196 Heki and Enomoto (2015) reported significant positive TEC breaks (exceeding the
197 absolute 3.0 TECU/h and relative 75% threshold) before five of eight Mw 8–9
198 earthquakes. We evaluate the probability of the case where the breaks are observed within
199 90 min before an earthquake assuming a Poisson process. The probability of observing n
200 events during a time period when μ events occur is expressed as follows:

201 $$f(n) = \frac{\mu^n}{n!} e^{-\mu}. \quad (3)$$

202 For example, when a 30° elevation mask angle is assumed, the average occurrence
203 rate is 0.76 times per 90 min (μ = 0.76) and the probability of observing at least one event

204 during the time period is $1 - f(0) = 53\%$. Figure 3d shows the probability calculated for
205 various elevation mask angles. With higher or lower elevation mask angles of 35° or 25°,
206 the probability decreases or increases to 39% or 62%, respectively. The Heki and
207 Enomoto (2015)'s 62% detection rate of the pre-seismic positive TEC breaks (five of the
208 eight great earthquakes) corresponds to our estimated probability with 25° elevation mask
209 angle even though the earthquake number of eight is too low to be evaluated
210 stochastically. Regarding their actual elevation mask adopted to these earthquakes, they
211 included breaks at very low elevation angles such as 15° for the 2012 Mw8.6 North
212 Sumatra Earthquake. Then our 25° elevation mask angle is not too low to compare with
213 their results. As a consequence, we cannot rule out a possibility that the detection of the
214 positive TEC breaks before the five great earthquakes was not a precursor but a product
215 of chance.

216 **4.2 Correspondence between the pre-seismic and post-seismic TEC changes**

217 We next test the correspondence between the pre-seismic and post-seismic TEC
218 changes reported by Heki and Enomoto (2013), where they proposed a temporal TEC
219 variation model, with the post-seismic drop representing a recovery from the pre-seismic
220 increase (as opposed to a net decrease). We follow their analysis by testing the correlation
221 between the pre-seismic increase and post-seismic decrease in the VTEC time series
222 around the source area. They modeled the VTEC time series from satellite PRN26 during
223 the 3-h period surrounding the mainshock, which consisted of four lines connected by
224 three breaks (Figure 4a; same as figure 3a in Heki and Enomoto (2013), but with the data
225 analyzed using our procedure). They assumed that period A represented the background
226 steady decrease in afternoon VTEC. Periods B and C correspond to the pre-seismic
227 increase and co-seismic decrease, respectively. They compared the integrated changes
228 during B and C relative to the trend during A, and found that the increase in B was
229 comparable to the decrease in C, which led them to report no net post-seismic VTEC
230 decrease (Heki and Enomoto, 2013). However, their analysis only incorporated seven
231 GNSS stations that were approximately aligned. We extend the GNSS station coverage to
232 test the spatial distribution of the VTEC changes. Figure 4b shows the relationship
233 between the two quantities for the broad GNSS station distribution shown in the map.

234 This result indicates that the coincidence between the increase and decrease is not
235 universal across the region, but rather limited to the stations selected by Heki and
236 Enomoto (2013). The spatial distributions of the increase and the decrease during periods
237 B and C, respectively, exhibit notably different patterns (Figures 4c and 4d).

238 This demonstration was prepared by Heki and Enomoto (2013) to respond to the
239 criticism by Kamogawa and Kakinami (2013) that the pre-seismic increase is an artifact
240 as a result of the post-seismic drop (tsunamigenic hole). Now a part of their rebuttal
241 seems invalid and we have to reconsider the possibility that the criticism by Kamogawa
242 and Kakinami (2013) is reasonable.

243 **4.3 Propagation of the TEC enhancement**

244 Heki and Enomoto (2013) has already pointed out that a LSTID, which traveled at
245 ~0.3 km/s from north to south and arrived at the source area ~1 h before the mainshock,
246 can provide one potential explanation for the TEC enhancement before the Tohoku-Oki
247 Earthquake. However, Heki and Enomoto (2015) showed that the appearance of the
248 breaks within the latitude range of the ruptured fault area is simultaneous, and then
249 suggested that the signatures of the breaks differ from that due to space weather. Figure
250 5a shows the arrival time distribution of the TEC breaks for satellite PRN15. The break is
251 represented by the –ΔAIC peak, which propagates from north to south, with a temporary
252 acceleration seen around 04:50 UTC above the source region of the Tohoku-Oki
253 Earthquake. This acceleration corresponds to the reported simultaneous enhancement.
254 However, these accelerations/decelerations often occur during LSTID propagation, such
255 that the LSTID propagation is not necessarily constant in velocity and direction. Figures
256 5b and 5c, and Movie S1 show the –ΔAIC propagation on the day of the Tohoku-Oki
257 Earthquake (DOY70) and the previous day (DOY69). The positive/negative breaks
258 change the propagation velocity, and frequently appear and disappear during the LSTID
259 propagation, as their nature. For example, positive breaks appear simultaneously even on
260 DOY69 (from 35 to 37°N around 05:40 UTC). This indicates that the acceleration of the
261 positive TEC break is not a special phenomenon and also not significant as an evidence
262 for its seismic origin.

4.4 Spatio-temporal distribution of post-seismic VTEC depletion

A large post-seismic TEC depletion was observed around the source region at the time of the Tohoku-Oki Earthquake, as reported from observations (e.g., Saito et al., 2011; Kakinami et al., 2012) and numerical models (Shinagawa et al., 2013). Here we analyze this post-seismic depletion from a spatiotemporal perspective.

We correct the inter-trace biases (ITBs) due to the ambiguity of the code pseudo range, as mentioned in the Appendix, to observe the faint spatial variations in the VTEC time series. Figure 6 shows the spatial distribution of the corrected VTECs for satellite PRN26 and PRN15, whose SIPs pass through the large-slip area around the time of the mainshock. A round-shaped hole is seen around the epicenter, even 54 min after the earthquake with PRN26 (Figure 6b). The TEC values at the center of the depletion area are ~5 TECU less than those of the surrounding area. The PRN15 also shows significant TEC depletion after the mainshock around the source area (Figures 6d and 6e). The post-seismic depletion can be seen more significantly in the movies. Movie S2 shows the pre- and post-seismic TEC variations at a 30-s sampling interval. The movie indicates that the first significant co-seismic disturbance (CID) appears above the source area at 05:55 UTC for satellite PRN26, which is ~9 min after the mainshock. This CID propagation has been reported by many papers (e.g. Tsugawa et al. 2011; Astafeyva et al. 2011; Kakinami et al. 2012). At least four positive peaks, each with a different velocity, propagate from the source region to the southwest and to the north, with the amplitude of the first wave being especially large. A hole that is centered at the radiant point of the CID emerges at around 06:05 UTC, after these peaks propagated across the area. Four other satellites also show a post-seismic hole, even though its outline is not as sharp as that observed with satellite PRN26 because their SIPs are not just above the large slip area at the moment of the mainshock (Movie S3). Movie S3 shows that post-seismic VTEC depletion is observed, even 120 min after the mainshock, and extends at least 500 km around the high-slip area for all of the satellites in view (PRN9, 15, 12, and 27). The spatial extent of the depletion area is not necessarily isotropic, but rather elongate in the northwest direction from the radiant point, which may reflect the alignment of the lifted area along the trench.

He and Heki (2016) studied the three-dimensional distribution of the ionospheric anomalies prior to three large earthquakes in Chile (Mw8.2, 8.4, 8.8). They modeled the

VTEC curves with the polynomials of time with degrees 3–5, excluding the intervals from the onsets of the anomalies detected using AIC to 20 minutes after the earthquakes. However, the 20 minutes is too short and their result is in danger of mistaking a large and long-lasting post-seismic depletion for a pre-seismic enhancement. This should be also the case of He and Heki (2018) which conducted three-dimensional tomography of ionospheric anomaly before the 2015 Illapel earthquake. They calculated STEC residual using excluding window whose start was given by the –ΔAIC and the ending time was assigned 25 minutes after the earthquake. He and Heki (2017) also studied the pre-seismic TEC enhancement before M 7–8 earthquakes using the reference curves, and claimed that these depletions should be limited spatially above the focal area, even if post-seismic holes exist, such that excluding the approximately ±30-min window around the earthquake is enough to avoid these effects since the IPP passes through the area within this period. However, they must have considered the temporal and spatial extent of the post-seismic depletion more carefully when adopting the window of data to exclude. The spatial extent of the depleted area could be wider than their assumption. We should evaluate it with the actual data or at least numerical simulation like Shinagawa et al. (2013).

5 Conclusions

We stochastically evaluated the occurrence rate of the positive TEC breaks proposed by Heki and Enomoto (2015) using the same procedure and threshold as in their study. Our averaged occurrence rate of TEC enhancement was much larger than that reported by Heki and Enomoto (2015) since we used all of the visible GPS satellites at GNSS station 3009. We detected 198 positive breaks within the 305-h time period using a 25° elevation mask angle. This corresponds to 62% probability that at least one positive break occurs within a given 90-min period assuming a Poisson process. Therefore, we cannot rule out the possibility that the pre-seismic VTEC changes, detected using the same procedure and threshold within 90 min before the 2011 Tohoku-Oki Earthquake and the other four great earthquakes, are just a product of chance.

We also studied spatio-temporal characteristics of the TEC break to find that the positive/negative breaks often change the propagation velocity and even appear and disappear

during the LSTID propagation as their nature. This suggests that the acceleration of the positive TEC break proposed by Heki and Enomoto (2015) is not a special phenomenon and also not significant as an evidence for its seismic origin.

We also analyzed the spatial distribution of the post-seismic TEC depletion for the Tohoku-Oki Earthquake with the data after reducing inter-trace biases. A significant post-seismic depletion that lasted at least 2 h after the earthquake and extended at least 500 km around the center of the large-slip area was observed. This means that evaluation of the enhancements using the reference curves with the short excluding time window which was adopted by Heki (2011) and even by the recent papers (e.g. He and Heki 2016, 2017, 2018) is in danger of mistaking a large and long-lasting post-seismic depletion for a pre-seismic enhancement. We cannot conclude that the TEC enhancements that Heki (2011) and the following papers have reported are not true precursors just by this observation of the Tohoku-Oki earthquake case and the stochastic evaluation. However, we cannot find any positive materials supporting their idea that the TEC enhancements are seismic origin.

Appendix： Inter-trace bias (ITB) corrction

The TEC traces still show biases of up to a few TECU, even between adjacent stations, after correcting the DCBs and IFBs for the satellites and stations, respectively. An example of the VTEC distribution at a moment for PRN15 is shown in Figure A1a. A random variation up to a few TECU is seen in the residual distribution after the local spatial averages are subtracted from the VTEC. A pair of STEC traces with a common satellite will show almost constant bias during a period when the satellite is continuously visible. We recognize these biases as ITBs, which should arise from uncertainties in the code pseudo range. The pseudo range has large variances up to a few TECU, as well as a drift bias that cannot be fit very well by the L4 shift (as described in section 2-1), even though the pseudo range is free of integer ambiguity. We therefore need to correct the ITB to study the faint spatial variation in TEC. We estimate the ITB based on the spatial average of the VTEC every hour. We define $VTEC_{ave\,ij}$ for the i-th station and the j-th satellite by the weighted average of the measured VTEC as follows:

$$VTEC_{pre\,ij}(t) = \frac{\sum_{m\neq i} VTEC_{mj}(t)\exp(-\frac{r_{mi}}{D})}{\sum_{m\neq i}\exp(-\frac{r_{mi}}{D})}, \quad (4)$$

where r is the horizontal distance from the SIP to the grid point at location (x, y) and D is the decay distance, which is set to 20 km. The summation is done for the stations within 60 km of the i-th station. One ITB is estimated for the trace of each satellite–station pair as the residual between the observed and predicted VTEC:

$$ITB_{ij} = \frac{1}{l}\sum_{n=1}^{l} \frac{\{VTEC_{ij}(t_n) - VTEC_{pre\,ij}(t_n)\}}{cos\psi_{ij}(t_n)}, \quad (5)$$

where l is the number of hours in the trace. To deduce the $VTEC_{pre\,ij}$, we select the stations that possess a residual of less than 3 TECU from $VTEC_{pre\,mj}$ for a robust estimation of $VTEC_{pre\,ij}$. We excluded 06:00 UTC during the ITB estimation to avoid the affect of the CID, which starts around 05:55. Each trace generally continues for 1–5 h. We finally obtain the corrected VTEC time series by subtracting $ITB_{ij}cos\psi_{ij}(t)$ from the initial VTEC time series.

Acknowledgments

All GPS data were downloaded from Geospatial Information Authority of Japan (https://terras.gsi.go.jp/). We acknowledge Dr. T. Sakai at the Electronic Navigation Research Institute (https://www.enri.go.jp/) and the University of Bern (ftp://ftp.aiub.unibe.ch/) for providing the receiver IFBs and satellite DCBs, respectively. We thank K. Heki and an anonymous reviewer for their critical and constructive comments.

References

Astafeyva, E., Lognonne P., & Rolland, L. (2011), First ionospheric images of the seismic fault slip on the example of the Tohoku-oki earthquake, *Geophysical Research Letters*, 38, L22104.

Heki, K. (2011), Ionospheric electron enhancement preceding the 2011 Tohoku-Oki earthquake, *Geophysical Research Letters*, 38, L17312.

Heki, K. & Enomoto, Y. (2013), Preseismic ionospheric electron enhancements revisited, *Journal of Geophysical Research, Space Physics*, 118, 6618–6626, doi:10.1002/jgra.50578.

Heki, K. & Enomoto, Y. (2015), M_w dependence of pre-seismic ionospheric electron enhancements, *Journal of Geophysical Research, Space Physics, 120*, 7006-7020.

He, L. & Heki, K. (2016), Three-dimensional distribution of ionospheric anomalies prior to three large earthquakes in Chile, *Geophysical Research Letters*, *43*, 7287-7293.

He, L. & Heki, K. (2017), Ionospheric anomalies immediately before M_w 7.0-8.0 earthquakes, *Journal of Geophysical Research, Space Physics*,*122*, 8659–8678.

He, L. & Heki, K. (2018), Three-dimensional tomography of ionospheric anomalies immediately before the 2015 Illapel earthquake, central Chile, *Journal of Geophysical Research, Space Physics*, 123, 4015–4025. https://doi.org/10.1029/2017JA024871

Ikuta, R., Satomura, M., Shimada, S., Fujita, A. & Ando, M. (2012), A small persistent locked area associated with the 2011 Mw9.0 Tohoku-Oki earthquake, deduced from GPS data, *Journal of Geophysical Research, Solid Earth*, 117, B11408, doi:10.1029/2012JB009335

Kakinami, Y., Kamogawa, M., Tanioka, Y., Watanabe, S., Gusman, A. R., Liu J-Y., Watanabe, Y., & Mogi, T. (2012), Tsunamigenic ionospheric hole, *Geophysical Research Letters*, 39, L00G27, doi:10.1029/2011GL050159.

Kamogawa, M. & Kakinami, Y. (2013), Is an ionospheric electron enhancement preceding the 2011 Tohoku-oki earthquake a precursor?, *Journal of Geophysical Research, Space Physics, 118*, 1-4, doi:10.1002/jgra.50118.

Masci, F., Thomas, J.N., Villani, F., Secan, J.A., & Rivera, N. (2015), On the onset of ionospheric precursors 40 min before strong earthquakes, *Journal of Geophysical Research, Space Physics*, 120, 1383–1393, doi:10.1002/2014JA020822.

Saito, A., Tsugawa, T., Otsuka, Y., Nishioka, M., Iyemori, T., Matsumura, M., Saito, S., Chen, C. H., Goi, Y. & Choosakul, N. (2011), Acoustic resonance and plasma depletion detected by GPS total electron content observation after the 2011 off the Pacific coast of Tohoku Earthquake, *Earth, Planets and Space*, 63, 863–867.

Sakai, T. (2005), Bias error calibration for observing ionosphere by GPS network, *IEICE Transactions on Communications*, J88-B, 2382–2389, (in Japanese).

Shinagawa, H., Tsugawa, T., Matsumura, M., Iyemori, T., Saito, A., Maruyama, T., Jin, H., Nishioka, M., & Otsuka, Y. (2013), Two-dimensional simulation of ionospheric variations in the vicinity of the epicenter of the Tohoku-oki earthquake on 11 March 2011, *Geophysical Research Letters*, 40, 5009–5013, doi:10.1002/2013GL057627.

Tsugawa, T., Saito, A., Otsuka, Y., Nishioka, M., Maruyama, T., Kato, H., Nagatsuma, T., & Murata, K. T. (2011), Ionospheric disturbances detected by GPS total electron content

observation after the 2011 off the Pacific coast of Tohoku Earthquake, *Earth, Planets and Space*, 63, 875–879.

Figure 1. VTEC time series for the three-week period surrounding the 2011 Tohoku-Oki Earthquake (same dataset as used in making figure 6 of Heki and Enomoto (2015)) for the same satellite (PRN15)–GNSS station (3009) pair. (a–c) VTEC time series. The red sections represent significant positive breaks (±30-min time window) that exceed 3 TECU/h and 75% of the original rate. The gray sections shortly after the Tohoku-Oki Earthquake also represent positive breaks but not counted considering post-seismic variation. (d–f) –□AIC calculated for (a)–(c), respectively.

Figure 2. Frequency of positive TEC breaks during the 61-day period. (a) Number of positive breaks in calendar time, with an elevation mask angle of 25°. The number at the top of each cell is the day of year. The small numbers in the day 040 cell denote the five 1-h periods, which span from 03:00 to 08:00 UTC. The colors indicate the number of detected breaks in each 1-h period. (b) Frequency of satellites in view that detected a positive break, with an elevation mask angle of 25°. The white bars show the number of satellites in view when a positive break is detected. The black bars show the number of satellites that simultaneously detected a break. (c) Frequency of positive TEC breaks as a function of time of day during the 61-day period. The blue bars indicate the cumulative number of positive TEC break events that were detected during each hour. The solid line shows the 61-day-averaged VTEC time series. The shaded magenta region highlights the time of day that was the focus of the analysis in (a) and (b) (03:00–08:00 UTC).

Figure 3. (a) Number of detected events and satellites in view against various elevation mask angles. (b) Number of events detected within the 61-day period (cyan) and average number of satellites in view (magenta) for a range of elevation mask angles. (c) Number of detected positive break events divided by the number of satellites in view. The expected number of events per satellite is approximately constant when the elevation mask angle is larger than 35°. (d) Probability of observing at least one break within a given 90 minutes assuming a Poisson process with different elevation mask angles.

Figure 4. (a) VTEC time series from satellite PRN26 at seven GPS stations with various focal distances from the Tohoku-Oki Earthquake epicenter. The ~3-h period surrounding the mainshock (marked by the vertical gray line), spanning from 03:45 UTC (2 h before the

446 earthquake) to 06:25 UTC (~40 min after the earthquake), is divided into four segments (marked
447 by the vertical red lines), which represent the (A) normal background, (B) precursory
448 enhancement, (C) co-seismic drop, and (D) post-seismic periods, and a linear fit to each segment
449 is determined (gray line segments). This figure is the same as figure 3a in Heki and Enomoto
450 (2013), with the exception of the estimated VTEC time series used here. (b) Difference between
451 the period B increase and period C decrease. The stations that were used by Heki and Enomoto
452 (2013) are indicated by circles with thick lines. The error bars denote 1σ uncertainties. The
453 observed difference is shown by the marker color. This figure is the same as figure 3c in Heki
454 and Enomoto (2013), with the exception of the additional stations used in the analysis. (c) Spatial
455 distribution of the degree of pre-seismic increase during period B at the stations. (d) Spatial
456 distribution of the degree of post-seismic decrease during period C at the stations. (e) Spatial
457 distribution of the difference between the period B increase and period C decrease. The stations
458 used by Heki and Enomoto (2013) are indicated by the larger circles with thick lines.
459

460 **Figure 5.** (a) Arrival time of the TEC break in the ±30-min window about the mainshock (05:46
461 UTC). The circles show the SIPs for satellite PRN15 at the time of the peak –ΔAIC value, whose
462 slope is larger than the threshold (3.0 TECU/h and 75%), which represents the positive TEC
463 break. The contours show the arrival time in 10-min intervals. The thick blue line marks the
464 Japan Trench, and the star shows the epicenter of the 2011 Tohoku-Oki Earthquake. The area
465 enclosed by the thin blue line is the large-slip area (>10 m) that was determined by Ikuta et al.
466 (2012). The rectangle extending from 35 to 45°N shows the area of the selected stations that was
467 used to depict the –ΔAIC propagation in Figures 5b and 5c. (b) –ΔAIC propagation among the
468 selected stations for satellite PRN15 before the Tohoku-Oki Earthquake (05:46 UTC on DOY70).
469 The circles with black and white edges indicate the positive and negative breaks, respectively,
470 for –ΔAIC values larger than 300. The vertical black line marks the time of the mainshock. The
471 vertical gray line denotes 05:23 UTC, which corresponds the start of the 30-min window, which
472 includes the co-seismic disturbance (CID) starting at 05:53 UTC. The white ellipse around 04:40
473 UTC shows the acceleration of the LSTID propagation (a positive break), which Heki and
474 Enomoto (2015) highlighted as a simultaneous appearance. (c) Same as Figure 5b, but for the
475 previous day (DOY69). The white ellipse around 05:40 UTC shows the acceleration of the
476 LSTID propagation (a positive break).
477
478 **Figure 6.** Absolute VTEC distribution with elevation mask angle of 20 degrees. Satellite PRN26
479 at (a) 05:40, (b) 06:40 UTC, and satellite PRN15 at (c) 05:40, (d) 06:40, and (e) 07:00 UTC on
480 March 11, 2011. The dots are color-coded to show the absolute VTEC value for each IPP
481 location at 300 km height. The thick black line shows the contour of the value 3 TECU larger
482 than the lowest value for each time. The thick blue line shows the Japan Trench, and the red star
483 shows the epicenter of the 2011 Tohoku-Oki Earthquake. The area enclosed by the thin blue line
484 is the large-slip area (>10 m) that was determined by Ikuta et al. (2012). The times in parentheses
485 indicate the lapse times relative to the mainshock.
486
487 **Figure A1.** VTEC distribution before and after the correction with PRN15 satellite at 7:20UT
488 (1h34m after the mainshock). (a) VTEC residual from the local spatial average before the
489 correction. The dots are color-coded to show the VTEC residual value for each IPP location at
490 300 km height. Imposed panel show the absolute VTEC. (b) Same with Figure A1a but after the

491 correction. The color scale for the main and the imposed panels are common with that in Figure
492 A1a.

Figure 1.

(a)

Day 053

10TECU

054

055

056

057

058

059

VTEC change

(b)

Day 060

061

062

063

064

065

066

(c)

Day 067

068

069

Tohoku-Oki Eq.

070

071

072

073

(d)

200

053
054
055
056
057
058
059

-ΔAIC

5 6 7 8 9

Time [UTC]

(e)

060
061
062
063
064
065
066

5 6 7 8

Time [UTC]

(f)

067
068
069
070
071
072
073

4 5 6 7 8

Time [UTC]

Figure 2.

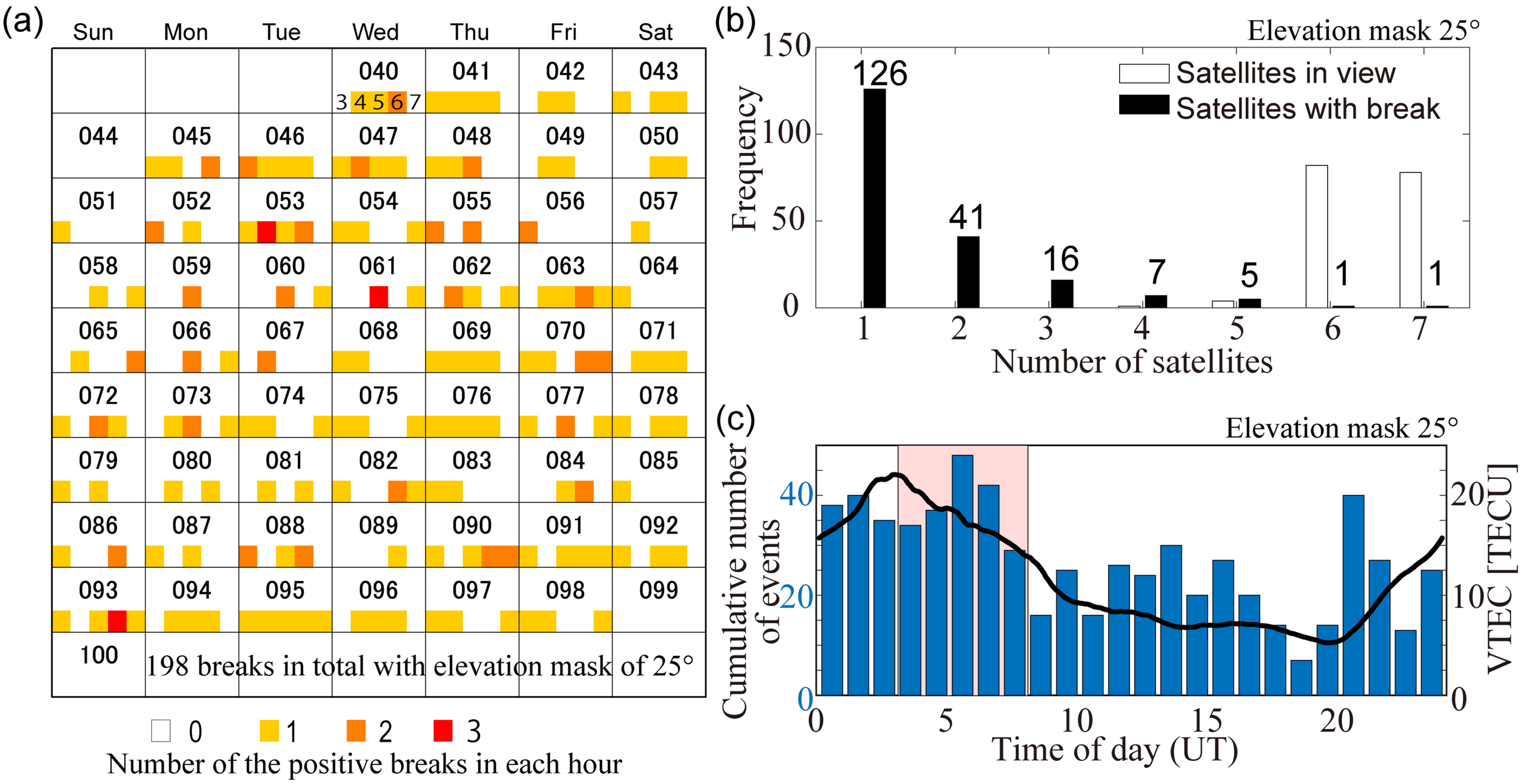
(a)
Sun
Mon
Tue
Wed
Thu
Fri
Sat
040
041
042
043
3 4 5 6 7
044
045
046
047
048
049
050
051
052
053
054
055
056
057
058
059
060
061
062
063
064
065
066
067
068
069
070
071
072
073
074
075
076
077
078
079
080
081
082
083
084
085
086
087
088
089
090
091
092
093
094
095
096
097
098
099
100
198 breaks in total with elevation mask of 25°
0
1
2
3
Number of the positive breaks in each hour
(b)
Elevation mask 25°
Satellites in view
Satellites with break
Frequency
150
100
50
0
126
41
16
7
5
1
1
1
2
3
4
5
6
7
Number of satellites
(c)
Elevation mask 25°
Cumulative number of events
40
20
0
20
10
0
VTEC [TECU]
0
5
10
15
20
Time of day (UT)

Figure 3.

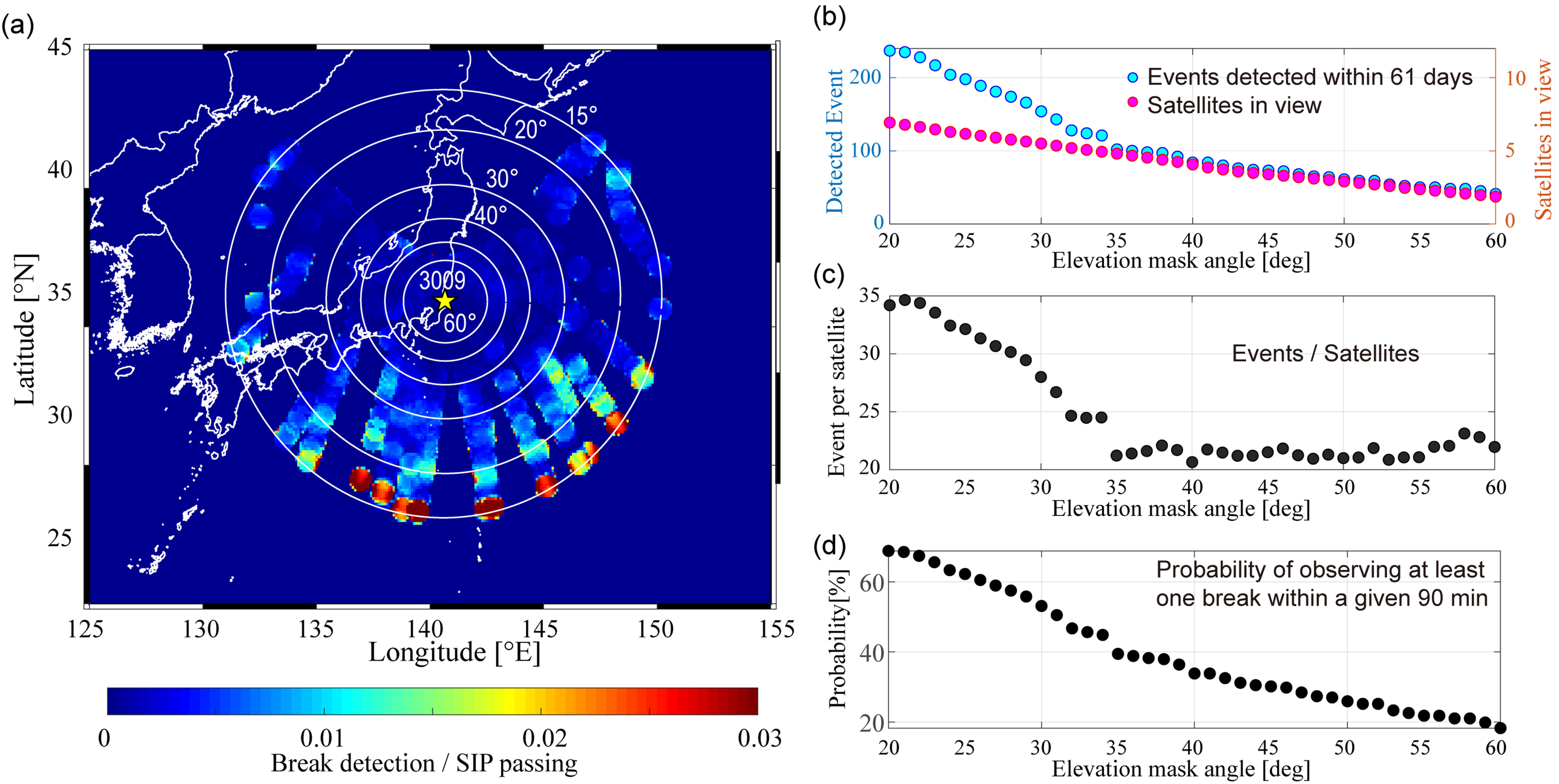
(a)
45
40
35
30
25
Latitude [°N]
125
130
135
140
145
150
155
Longitude [°E]
15°
20°
30°
40°
60°
3009
0
0.01
0.02
0.03
Break detection / SIP passing
(b)
Detected Event
200
100
0
Satellites in view
10
5
0
Events detected within 61 days
Satellites in view
20
25
30
35
40
45
50
55
60
Elevation mask angle [deg]
(c)
Event per satellite
35
30
25
20
Events / Satellites
Elevation mask angle [deg]
(d)
Probability[%]
60
40
20
Probability of observing at least
one break within a given 90 min
Elevation mask angle [deg]

Figure 4.

(a)

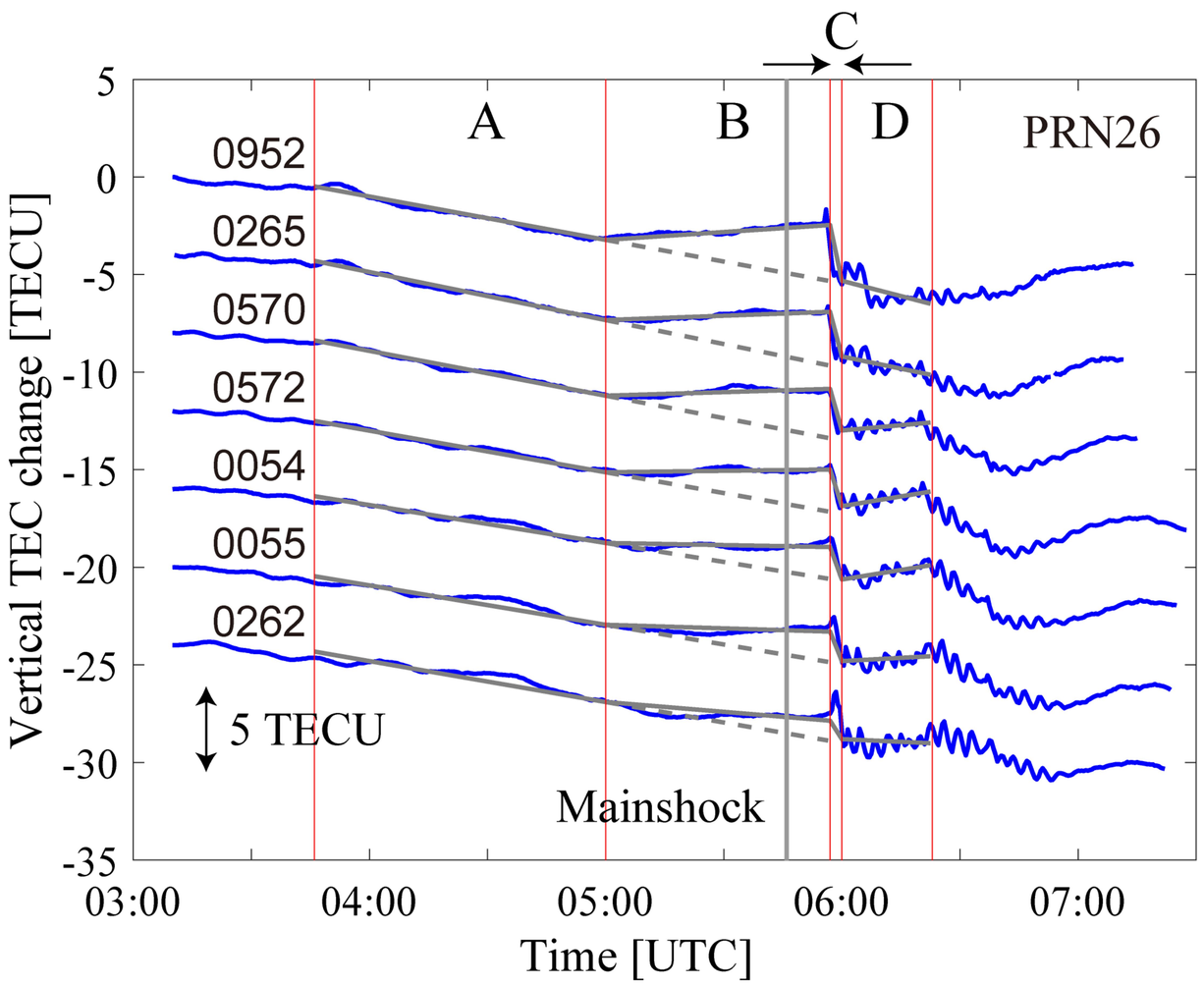
C
A
B
D
PRN26
0952
0265
0570
0572
0054
0055
0262
5 TECU
Mainshock
Vertical TEC change [TECU]
Time [UTC]
03:00
04:00
05:00
06:00
07:00
5
0
-5
-10
-15
-20
-25
-30
-35

(b)

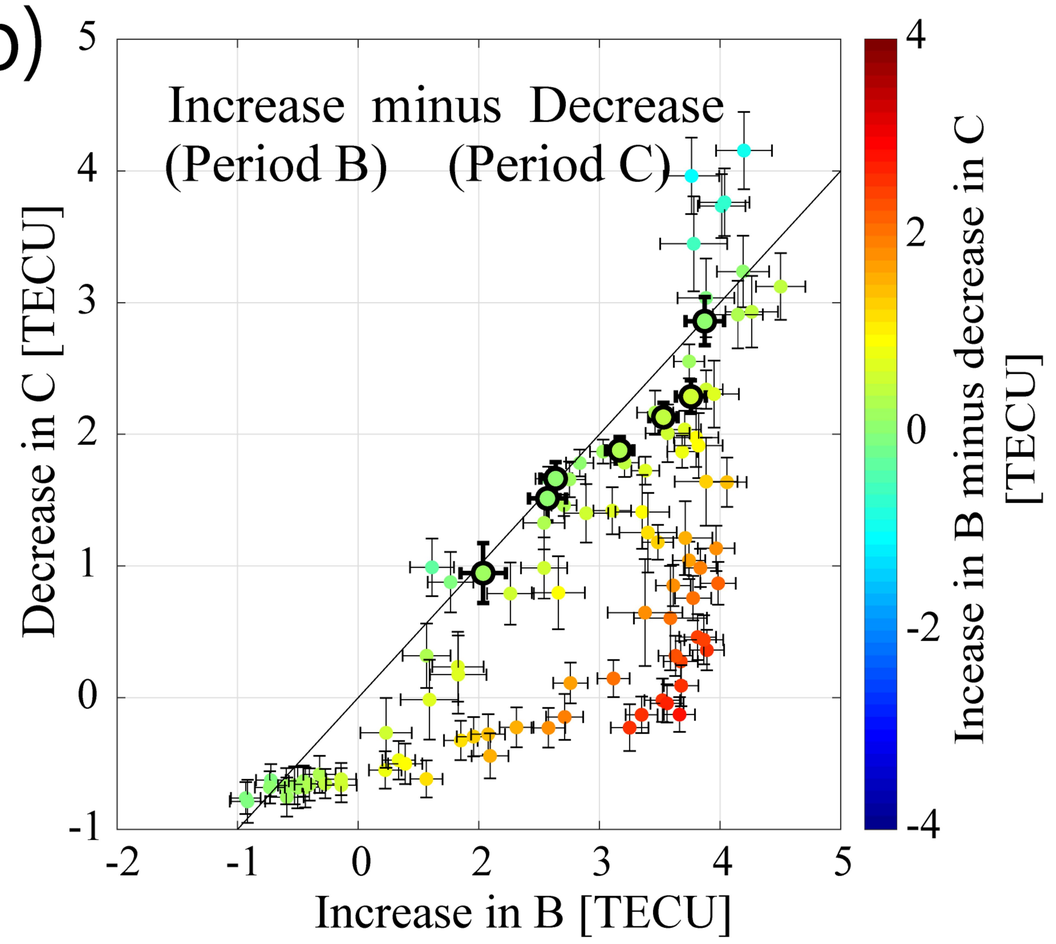
Increase minus Decrease
(Period B) (Period C)
Decrease in C [TECU]
Increase in B [TECU]
Incease in B minus decrease in C [TECU]
5
4
3
2
1
0
-1
-2
-4

(c)

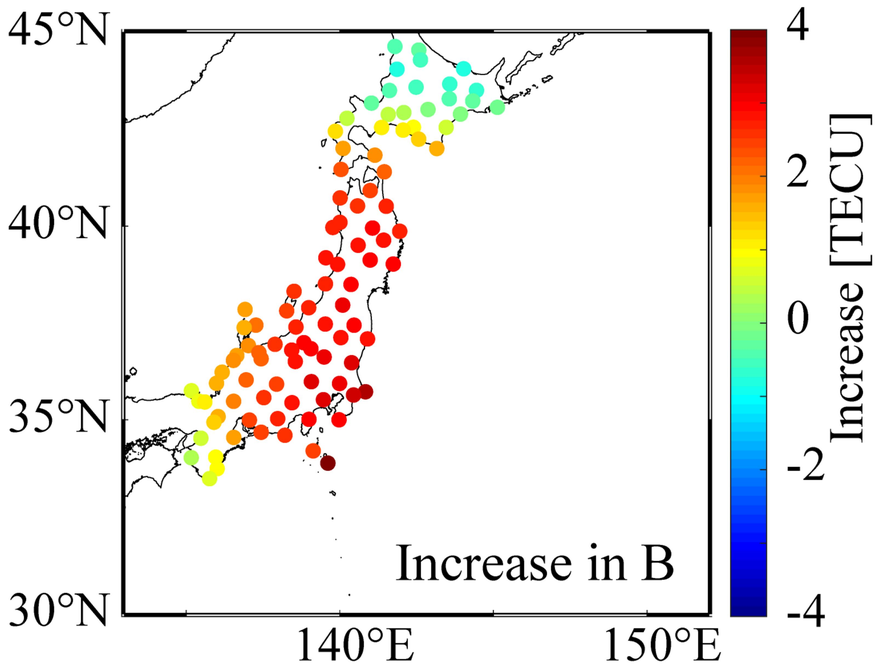
45°N
40°N
35°N
30°N
140°E
150°E
Increase in B
Increase [TECU]
4
2
0
-2
-4

(d)

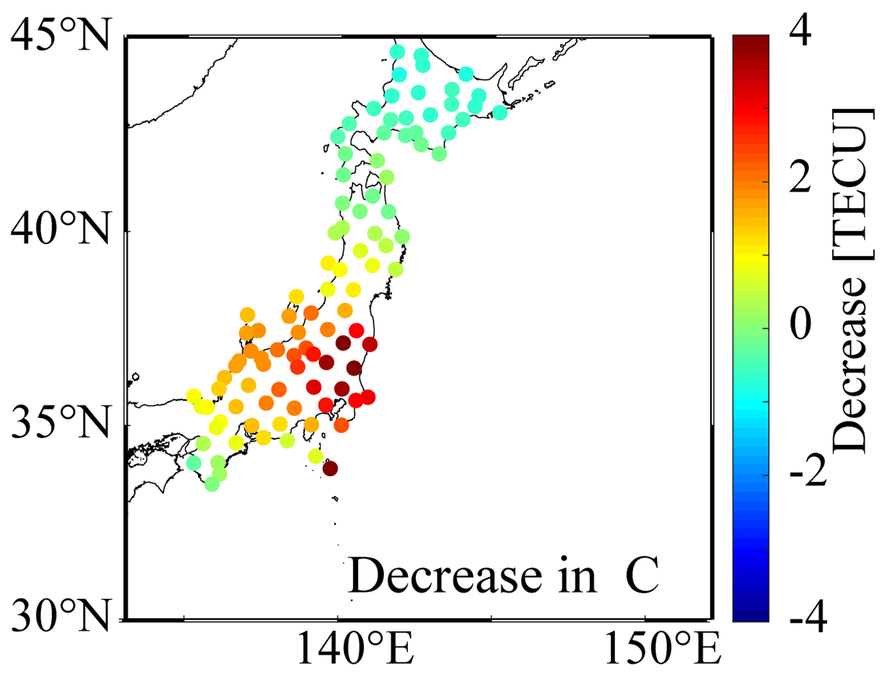
45°N
40°N
35°N
30°N
140°E
150°E
Decrease in C
Decrease [TECU]
4
2
0
-2
-4

(e)

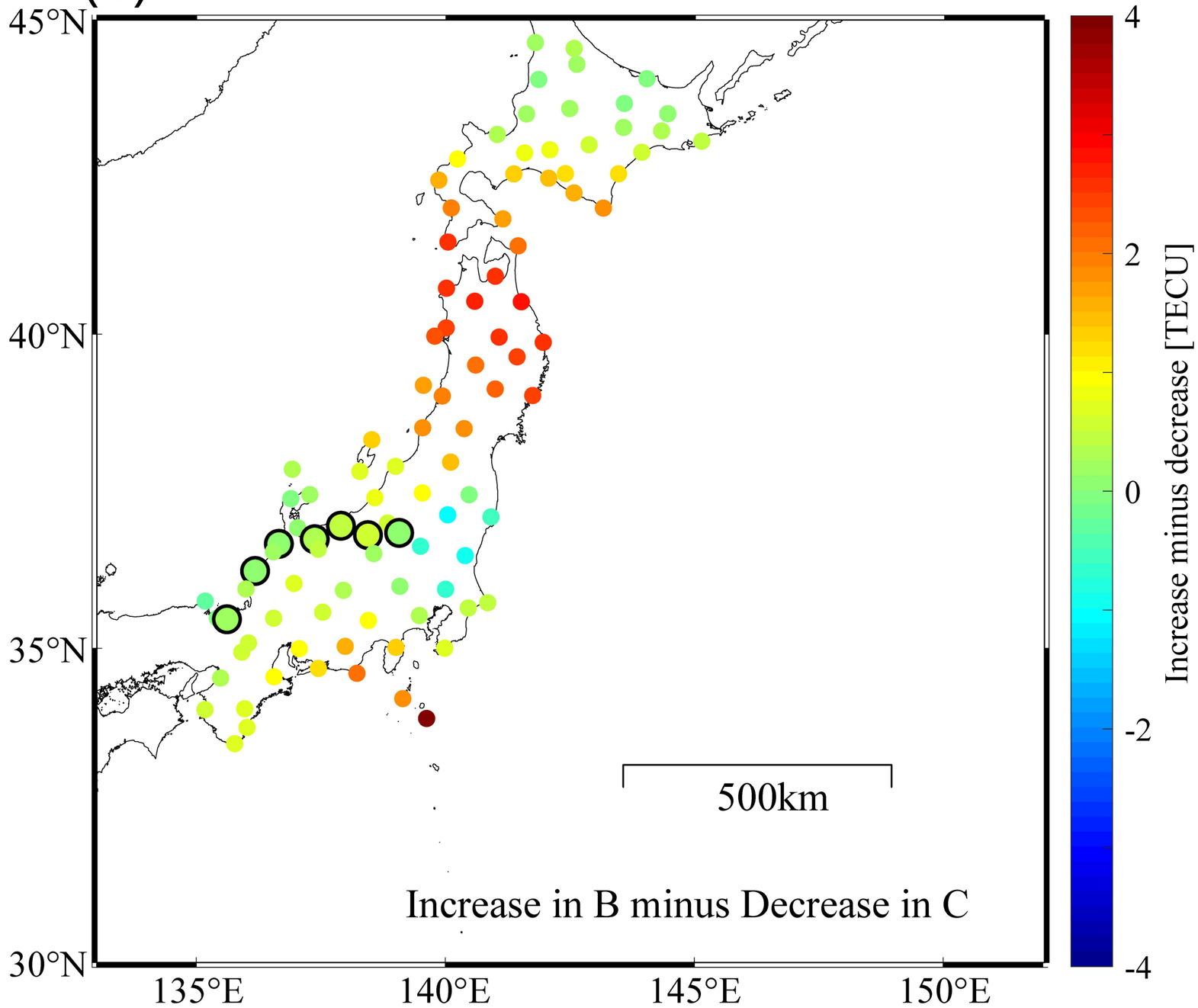
45°N
40°N
35°N
30°N
135°E
140°E
145°E
150°E
500km
Increase in B minus Decrease in C
Increase minus decrease [TECU]
4
2
0
-2
-4

Figure 5.

(a)

45°N
40°N
35°N
30°N
130°E
135°E
140°E
145°E
04:20
04:30
04:40
04:50
05:00
05:10
05:30
05:20
Mw9.0
(05:46)
500km
PRN15
06:00
05:45
05:31
05:16
05:02
04:48
04:33
04:19
04:04
03:50
Time (UTC)

(b)

SIP Latitude [°N]
46
44
42
40
38
36
34
32
DOY70
04:00
05:00
06:00
Time (UTC)
400
350
300
250
200
150
100
50
0
-ΔAIC

(c)

SIP Latitude [°N]
46
44
42
40
38
36
34
32
DOY69
04:00
05:00
06:00
Time (UTC)
400
350
300
250
200
150
100
50
0
-ΔAIC

Figure 6.

(a)

PRN 26

05:40 (−6 min)

(b)

PRN 26

06:40 (54 min)

45°N
40°N
35°N
30°N
135°E
140°E
145°E
500 km

VTEC [TECU]
40
35
30
25

(c)

PRN 15

05:40 (−6 min)

(d)

PRN 15

06:40 (54 min)

(e)

PRN 15

07:00 (74 min)

45°N
40°N
35°N
30°N
135°E
140°E
145°E
500 km

VTEC [TECU]
45
40
35

Figure A1.

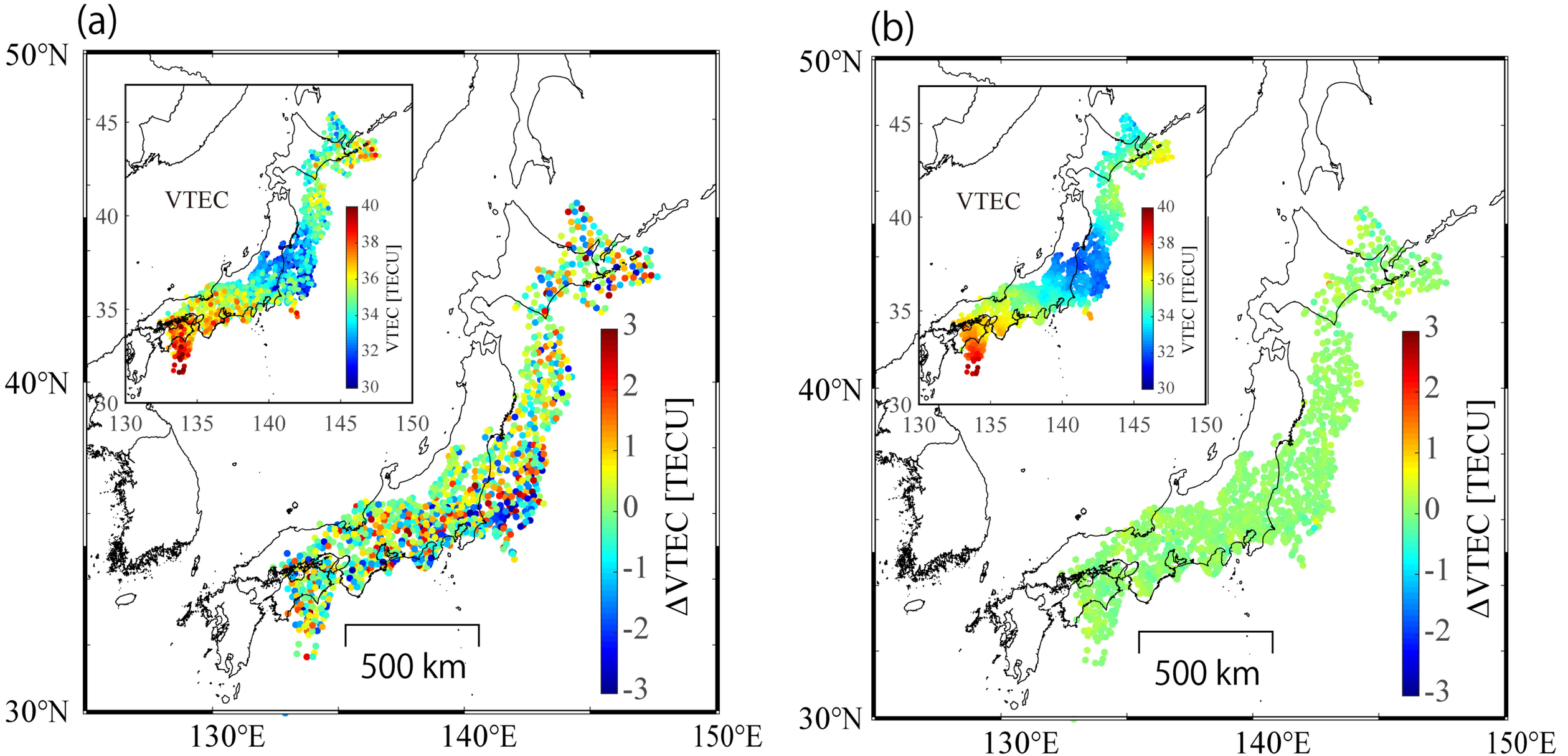
(a)
(b)
50°N
40°N
30°N
130°E
140°E
150°E
VTEC
VTEC [TECU]
ΔVTEC [TECU]
500 km